Enhanced superconducting transition temperatures in the rocksalt-type superconductors $In_{1-x}Sn_xTe$ ($x \leqslant 0.5$)

Kaya Kobayashi,[1,2] Yukio Ai,[2] Harald O. Jeschke,[1] and Jun Akimitsu[1]

[1]*Research Institute for Interdisciplinary Science, Okayama University, Okayama 700-8530, Japan*
[2]*Department of Physics, Okayama University, Okayama 700-8530, Japan*

We investigate superconductivity in $In_{1-x}Sn_xTe$ ($x \leqslant 0.5$) synthesized at high pressures of up to 2 GPa and observe an enhancement of the superconducting transition temperature T_c for increasing tin concentration x. These compounds have not been accessible in rocksalt structure via conventional ambient pressure synthesis. While the lattice constant smoothly increases with x, T_c saturates around $x = 0.4$. Electronic structure calculations indicate that the T_c modulation is brought on by the change of the density of states in the vicinity of the Fermi energy [$N(E_F)$]. However, differences between the calculated $N(E_F)$ and the observed electronic specific-heat coefficient indicate that the phonon dispersion plays an important role in the system and that the mechanism of superconductivity may not be the same in the entire doping range.

I. INTRODUCTION

Well-studied materials such as narrow gap semiconductors and semimetals are now regaining wide recognition, due to the topological classification of existing materials [1] and a growing number of studies on such new aspects. This has added a dimension to our way of organizing materials and brought out the rich field of topological insulators (TI) [2] and Dirac/Weyl semimetals [1]. A closely related class of materials which are often coexisting are topological superconductors (TSCs), where the superconducting gap plays the role of the band gap in which topological edge modes with exotic properties exist [3]. Despite intense interest, less is known experimentally about TSCs. Similar to the classification of TI, TSCs are also classified according to the topological invariant [4]. Among the most studied materials are intercalated narrow-gap semiconductors, such as $Cu_xBi_2Se_3$ [5,6], $Sr_xBi_2Se_3$ [7,8], and $Nb_xBi_2Se_3$ [9,10]. Another example is a doped topological crystalline insulator (TCI), SnTe [11–15]. Undoped stoichiometric SnTe has been known as a narrow-gap semiconductor and studied by tunneling experiment [16]. The topologically protected surface state is observed due to the mirror symmetry of the material [17] and survives in the superconducting state [18].

Nonstoichiometric $Sn_{1-x}Te$ was known to show superconductivity at low temperature [19] in addition to superconductivity induced in SnTe by doping Sb [19], Mn [20], In [15], and many other elements. Among various dopants, indium is known as an exceptionally effective dopant [15], which also suppresses the ferroelectric structural phase transition [11]. The dopant was discussed to have resonant states similar to Tl in PbTe in the perspective of how impurity states are formed in the ferroelectric compounds, limiting the mechanism to the shallow doping regime [21]. Recent studies show that the indium doping level in $In_{1-x}Sn_xTe$ can be varied between $1 - x = 0$ [11] and $1 - x = 0.4$ [13] while maintaining NaCl structure for all compositions in between [12]. Here we report the synthesis of compounds with higher In content, $In_{1-x}Sn_xTe$

($0 \leqslant x \leqslant 0.5$) and show that the superconductivity is enhanced when Sn is doped into NaCl structure InTe. We work out the relation to the change of density of states (DOS) in the vicinity of the Fermi level and discuss preliminary evidence for the possible role of phonons in the superconductivity.

II. EXPERIMENTAL METHODS

Stoichiometric amounts of 5N pure Te powders and 3N pure Sn (2–5 mm diameter), 4N pure In shots (3–6 mm diameter) were sealed in evacuated quartz tubes and heated to 850 °C for 24 h. Obtained crystals appear brown gray with metallic surface. The polycrystalline crystals show the existence of cubic SnTe and tetragonal InTe impurity as many previous studies of higher In doped in TCI SnTe report [12–14,22]. The obtained crystals were mixed thoroughly and the pelletized mixture was mounted at the center of high-pressure cells protected in a BN sheath. The cell is heated at 500 °C, 2 GPa for 30 m to give crystals of blue gray surface as was described in previous reports [23–25]. Powder x-ray diffraction (XRD) measurements were performed at room temperature using a Rigaku 1100 diffractometer with Cu Kα radiation to confirm the rocksalt type crystal structure. Electrical resistivity ρ and the specific heat C were measured with a Quantum Design Physical Property Measurement System (PPMS) and magnetic susceptibility χ measured with a Quantum Design Magnetic Property Measurement System (MPMS) under magnetic field $B = 1$ mT.

III. THEORETICAL METHODS

We employed density functional theory and used the full-potential local orbital (FPLO) code (versions 14.00-49 and 5.50-50) [26,27]. The generalized gradient approximation (GGA) in Perdew, Burke, Ernzerhof form was used for the exchange-correlation functional [28]. We converged the
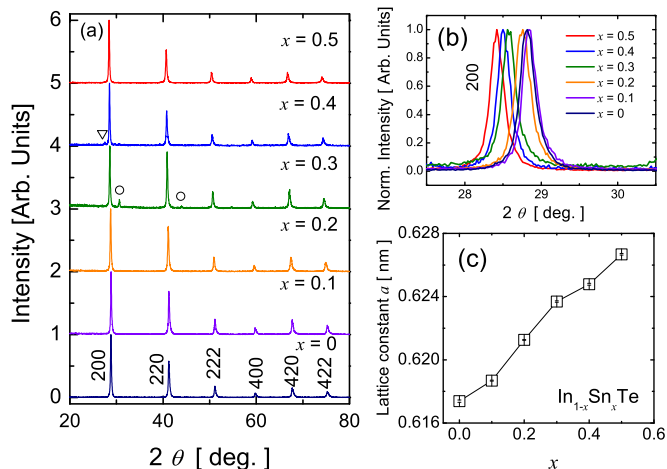
FIG. 1. (a) Powder x-ray diffraction patterns for $In_{1-x}Sn_xTe$ ($x = 0 \sim 0.5$). Peaks are indexed as shown in the lower part of the panel. Except for a BN peak for $x = 0.3$ ($\triangledown$) and small InTe peaks for 0.4 ($\bigcirc$), no impurity peaks were observed. (b) Normalized peak of (200) for $In_{1-x}Sn_xTe$ ($x = 0 \sim 0.5$). Increasing x brings the peak to lower θ, indicating the increasing lattice constant, a. (c) Lattice constant a increases when increasing Sn doping in InTe. The uncertainty of the lattice constant stays negligibly small for all x including those with impurity peaks ($x = 0.3$ and 0.4).

calculations on $100 \times 100 \times 100 \, k$ meshes for InTe and on $50 \times 50 \times 50 \, k$ meshes for all doped compounds.

IV. RESULTS AND DISCUSSION

Powder XRD patterns for $In_{1-x}Sn_xTe$ ($x = 0 \sim 0.5$) are shown in Fig. 1(a). A clear NaCl-type structure (space group $Fm\bar{3}m$) is observed for all compounds with a presence of diminutive impurity peaks for $x = 0.3$ and 0.4. An observed impurity peak for $x = 0.3$ is from the BN sheath in the pressure cell, and two peaks observed for $x = 0.4$ are from NaCl-type InTe. The normalized peak of (200) for $x = 0 \sim 0.5$ are depicted in Fig. 1(b). The monotonic shift toward lower angle 2θ indicates the increasing lattice constant, which is presented in Fig. 1(c). The overall dependence of the lattice constant a on x is an increase toward SnTe as depicted in Fig. 1(c). The linear relation connects smoothly with the previous report [12] as shown in the inset of Fig. 5.

In all samples of $In_{1-x}Sn_xTe$ ($x = 0 \sim 0.5$), the bulk superconductivity is confirmed by dc magnetic susceptibility χ measurements. Typical curves for $x = 0.5$ are shown in Fig. 2(b). We assign the superconducting transition temperature T_c to the T at which the linear fit to normal state and superconducting state crosses. A well-defined T_c can be obtained as seen in Fig. 2(b). The obtained T_cs are plotted against x in Fig. 2(a). The plot shows that T_c is enhanced upon Sn doping with rapid increase in the vicinity of $x = 0.2$, followed by a gradual saturation above $x = 0.4$. This behavior is different from that of In doping in isostructural SnTe [11,12]. We also performed magnetization measurements while sweeping the magnetic field B to obtain the lower critical field H_{c1}. H_{c1} is derived as an inflection point in magnetization curves $M(B)$ when increasing B below T_c. The obtained H_{c1} is plotted in the
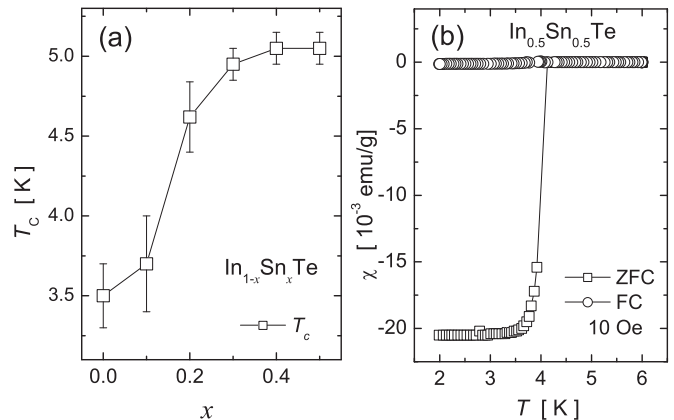

FIG. 2. (a) Superconducting transition temperatures (T_cs) obtained from the susceptibility measurement are plotted against Sn doping x in $In_{1-x}Sn_xTe$ ($x = 0 \sim 0.5$). T_c is enhanced by Sn doping and saturates above $x = 0.4$. Small doping levels show a variation of T_c between samples resulting in larger error bars. (b) Temperature dependence of susceptibility χ for $In_{0.5}Sn_{0.5}Te$. A clear T_c is obtained when the signal deviates from 0.

inset of Fig. 3(b). The data are well fitted using a parabolic T dependence, $H_{c1}(T) = H_{c1}(0)[1 - (T/T_c)^2]$, to give $H_{c1}(0)$ as 50.9(8) mT for $x = 0.3$, 25.7(3) mT for $x = 0.5$ and 25.5(0) mT for $x = 1$.

The resistivity ρ under several different magnetic fields B is measured for temperatures down to 2 K. The shift of T_c toward low T is shown in increasing B from 0 to 1.5 T in Fig. 3(a). The obtained upper critical field H_{c2} is plotted in Fig. 3(b). H_{c2} at $T = 0$, $H_{c2}(0)$ is derived using the Werthamer-Helfand-Hohenberg (WWH) equation [29], i.e., the slope at T_c, $\frac{dH_{c2}}{dT}|_{T=T_c}$ is proportional to $H_{c2}(0)$. A simple parabolic T dependence, $H_{c2}(T) = H_{c2}(0)[1 - (T/T_c)^2]$, well

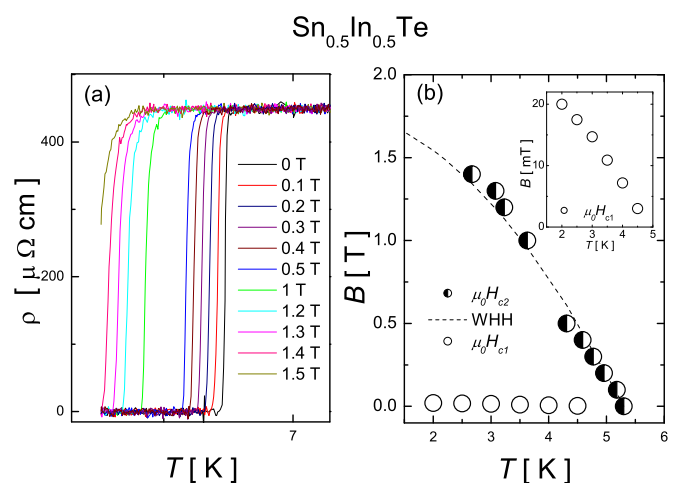FIG. 3. (a) Temperature dependence of the resistivity in various magnetic fields ($B = 0 \sim 1.5$ T) for $In_{0.5}Sn_{0.5}Te$. Gradual shift of superconducting transition T_c is observed when increasing B. (b) Obtained upper critical fields (H_{c2}) from ρ data presented in the left panel. The lower critical-field (H_{c1}) data is enlarged in the inset panel. H_{c2} is well described by the Werthamer-Helfand-Hohenberg equation (dashed line); for details see the text.

TABLE I. Superconducting parameters of cubic Sn-doped InTe and InTe. The T_c of $Sn_{0.5}In_{0.5}Te$ is derived from transport measurements while those of $Sn_{0.3}In_{0.7}Te$ and InTe are obtained from heat-capacity measurements.

Parameter	Units	$In_{0.5}Sn_{0.5}Te$	$In_{0.7}Sn_{0.3}Te$	InTe
$T_C(\chi)$	K	4.9(5)	5.1(0)	3.5(8)
$T_C(\rho)$	K	5.2(1)	5.2(8)	3.6(5)
$\mu_0 H_{c1}(0)$	mT	25.7(3)	50.9(8)	25.5(0)
$\mu_0 H_{c2}(0)$	T	2.0(0)	1.6(3)	0.1(1)
$\mu_0 H_c(0)$	mT	136.8(9)	194.2(1)	42.3(1)
$\xi(0)$	Å	128.(3)	142.(0)	542.(1)
$\lambda(0)$	nm	184.6(2)	118.7(1)	241.2(3)
$\kappa(0)$		14.39(1)	8.35(8)	4.4(5)
$\gamma(0)$	$\frac{mJ}{molK^2}$		3.92	4.69
$\frac{\Delta C}{\gamma T_c}$			3.24	1.90
Θ_D	K		129	131
λ_{ep}			0.94	0.78

reproduces the measured $H_{c2}(T)$ data. H_{c2} is shown as a broken line in Fig. 3(b), indicating that the obtained $H_{c2}(0)$ from WHH well describes the measured data. H_{c1} is a couple of orders of magnitude smaller than H_{c2}, indicating the existence of a large intermediate state in the material. H_{c2} does not show a large x dependence between $x = 0.3$ to 0.5, with $\mu_0 H_{c2}(0)$ being 1.63 and 2.0 T, respectively. H_{c2} in $In_{1-x}Sn_xTe$ ($x > 0$) is greatly increased compared to that of $x = 0$, where $\mu_0 H_{c2}(0) = 0.1$ T. The typical parameters obtained for these three compounds, $In_{1-x}Sn_xTe$ for $x = 0$, 0.3 and 0.5, are listed in Table I. The drastic change in $H_{c2}(0)$ by an order of magnitude is triggered by Sn doping, and is surprising when T_c and $H_{c1}(0)$ do not show a change of the same magnitude. This difference provides a strong motivation to look into the superconducting properties. Using $\mu_0 H_{c2}(0)$, we are able to estimate the coherence length $\xi(0) = (\phi_0/2\pi H_{c2})^{-1/2}$ listed in Table I. For $x = 0.3$ and 0.5, we obtained $\xi(0) = 142.0(9)$ and $128.3(0)$ Å, respectively, while for $x = 0$, it increases to $\xi(0) = 542.0(9)$ Å. This is not a monotonic dependence on x, if we include $\xi(0) \sim 150$ Å [12,13], or 154 Å at $x = 0.6$ in the comparison [14]. The penetration depth λ is also obtained from $H_{c1}(0)$ using the relation with $\xi(0)$, $H_{c1}(0) = \frac{\phi_0}{4\pi\lambda^2} \ln\frac{\lambda}{\xi}$. The obtained $\lambda(0)$ shows a decreasing behavior upon increase of the In ratio as presented in Table I until it bounces back to 133 nm in InTe. The very different evolution of $H_{c1}(0)$ and $H_{c2}(0)$ with Sn concentration x is an indication that the superconducting state is modified by the variation of the Sn/In ratio. The difference obtained in χ and ρ measurements listed in Table I is also observed in Refs. [11,12]. We note here that the difference between zero resistivity and the onset in the ρ curve is within 0.2 K, indicating that sample inhomogeneity is excluded.

To further elucidate the difference between superconductivity in InTe and Sn-doped InTe, we performed specific-heat C measurements on InTe and $In_{0.7}Sn_{0.3}Te$. Bulk SC transitions were observed for both compounds as shown in Fig. 4(a). The signal corresponding to a nonsuperconducting state is determined at $B = 3$ T and shown in Fig. 4(b). The curves for doped and undoped InTe look similar, as was expected
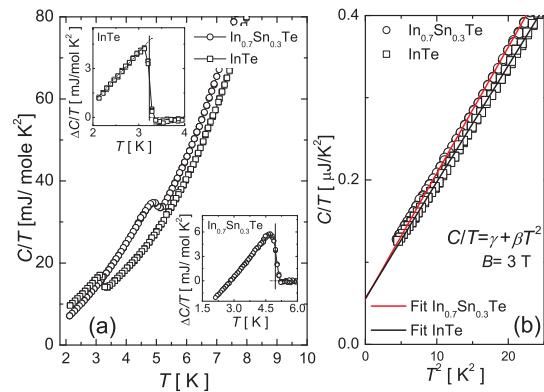

FIG. 4. (a) Heat-capacity analysis of $In_{0.7}Sn_{0.3}Te$ and InTe samples. The curves are measured without a magnetic field (B). Samples show $T_c = 4.99$ K ($In_{0.7}Sn_{0.3}Te$) and 3.2 K (InTe). The inset panels depict the ΔC to show the superconducting transitions in the heat capacity for both compounds. The magnitude of the jump at the transition depends on the doping level of Sn. (b) (Color online.) The heat capacity measured in $B = 3$ T for $In_{0.7}Sn_{0.3}Te$ and InTe. The well-fitting T^3 dependence is seen for two compounds with largely different TC. The fitted curves are depicted in red and black for $In_{0.7}Sn_{0.3}Te$ and InTe, respectively.

from T_c and H_{c2}. The C/T curves are fitted with a function of $C/T = \gamma + \beta T^2$. The phonon contribution to the heat capacity is determined by the coefficient β. β is related to the Debye temperature Θ_D through $\beta = nN_A\frac{12}{5}\pi^4R\Theta_D^{-3}$, where $R = 8.314$ J mol^{-1}K^{-1}, n is the number of atoms per formula unit, and N_A is Avogadro's number. We obtained $\Theta_D = 129$ K for $x = 0.3$ and 131 K for InTe. These fall into a similar range with In-doped SnTe superconductors that are in the vicinity of 200 K [12–14,22]. Thus we can compare them in detail; the change of Θ_D is listed in Table I. Θ_D is nearly constant when the Sn content in $In_{1-x}Sn_xTe$ is increased up to $x = 0.3$, which is different from the behavior of the Sn rich compound [12]; $\Theta_D = 204$ K for $In_{0.05}Sn_{0.95}Te$, and 162 K for $In_{0.4}Sn_{0.6}Te$. No strong suppression or enhancement associated with the T_c modulation is observed in the system, indicating that electron-phonon coupling enhancement plays only a small part in the modulation of T_c.

The parameter γ represents the distribution of electrons, and strongly relates to the DOS at the Fermi energy (E_F) as $\gamma = \pi^{3/2}k_B^2N(E_F)(1 + \lambda_{ep})$, where k_B is the Boltzmann constant, $N(E_F)$ is the DOS at E_F, and λ_{ep} is the coupling constant of electrons and phonons. The extracted $N(E_F)$ for $x = 0.3$ and 0 are listed in Table I. The behavior of $\gamma(0)$ [mJ mol^{-1} K^{-2}] is depicted in Fig. 5 along with the data extracted from the literature [12]. The previous reports indicate that the dopant In introduces charge carriers in the system [12,15] as well as DOS at E_F [12]. The authors of Ref. [12] argue that the dopant (In) forms a band in the vicinity of E_F, which effectively contributes to conductivity as a resonating state (the resonating state scenario) [12]. The x dependence of T_c in the range of $0 < x \leqslant 0.5$ does not show the same trend as in the range of $x \geqslant 0.6$. T_c is monotonically increasing up to 5.5 K at $x = 0.5$, then slowly decreases as Sn decreases in the system. The decrease of T_c indicates that the observed γ does not define
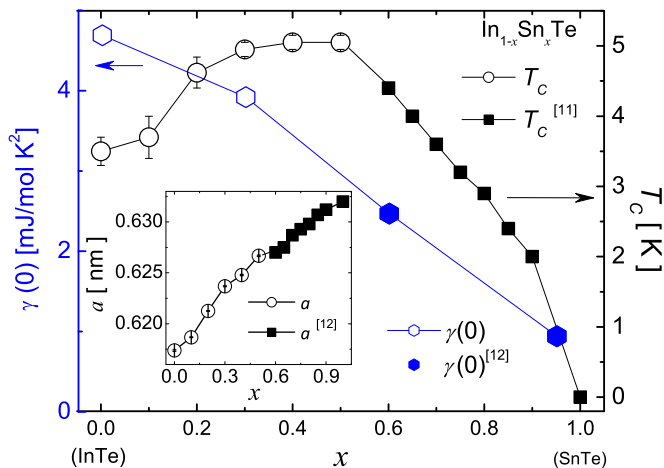
FIG. 5. x dependence of superconducting transition temperature and specific-heat coefficient. In the high x region, data is taken from a previous report [12] and depicted as filled symbols. TC is enhanced in the mixed state of Sn and In from both ends (SnTe and InTe). The change on the InTe side is gradual compared to the SnTe side. The obtained $\gamma(0)$ parameter is roughly proportional to the In ratio in the compounds, contrasting with the nonmonotonic change of TC.

the T_c and the resonating dopant scenario is not appropriate in the discussed region of x below 0.5.

We have performed electronic structure calculations for InTe in the $Fm\bar{3}m$ structure using the measured lattice constants [Fig. 6(a)]. We use the all-electron full-potential local orbital (FPLO) basis [26] and GGA exchange correlation
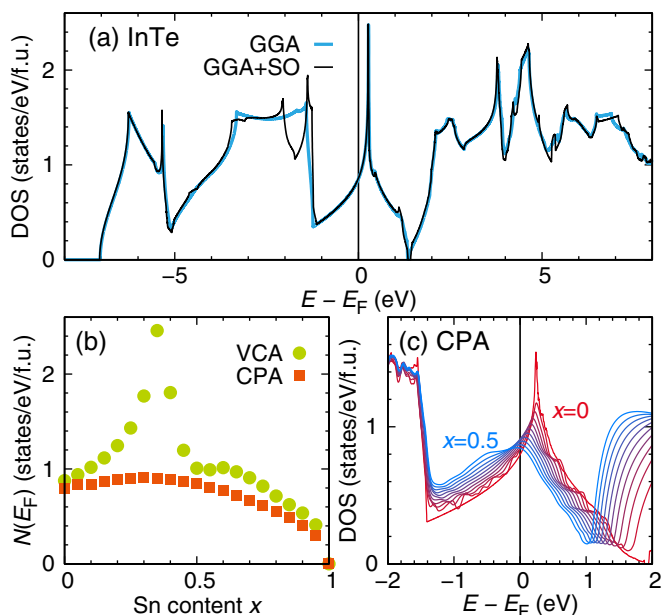

FIG. 6. Electronic structure of $In_{1-x}Sn_xTe$. (a) Comparison between scalar (GGA) and fully relativistic (GGA+SO) densities of states of pure InTe. (b) Evolution of the density of states at the Fermi level for $In_{1-x}Sn_xTe$ as function of x determined by virtual crystal approximation (VCA, circles) and coherent potential approximation (CPA, squares). (c) k-integrated spectral function from CPA for different Sn content x.

functional. We find that especially near the Fermi level, effects of spin-orbit coupling are small, as scalar and fully relativistic electronic structures are nearly identical. About 0.24 eV above the Fermi level, there is a sharp peak in the DOS, suggesting that electron doping of InTe could significantly increase the DOS at the Fermi level. This is confirmed when we use the virtual crystal approximation to simulate partial replacement of In by Sn; in this approximation, the nuclear charge of In is increased between 49 (In) and 50 (Sn), simulating a perfectly homogeneous $In_{1-x}Sn_xTe$ crystal. As expected, the density of states at the Fermi level increases sharply up to a spike at $x = 0.35$ before falling again abruptly [Fig. 6(b)]. However, this simulation does not take into account that partially replacing In by Sn introduces disorder into the crystal. Therefore, we use the coherent potential approximation (CPA) [27] to assess the effect of disorder in the $In_{1-x}Sn_xTe$ alloy. The results are the square symbols in Fig. 6(b). Due to disorder, the DOS only increases by 14% up to $x = 0.3$ before falling again. The reason can be understood from Fig. 6(c): The disorder introduced by increasing the amount of Sn in InTe broadens the features of the spectral function. Thus, rather than shifting the Fermi level towards the sharp peak above E_F, spectral weight is redistributed and only mild changes of $N(E_F)$ occur. This observation is in good qualitative agreement with the evolution of the T_c observed experimentally (Fig. 5).

We use the modified McMillan equation [30,31]

$$\lambda_{ep} = \frac{1.04 + \mu^* \ln(\Theta_D/1.45T_c)}{(1 - 0.62\mu^*)\ln(\Theta_D/1.45T_c) - 1.04} \quad (1)$$

to obtain a rough estimate of the electron-phonon coupling constant λ_{ep} using T_c and Θ_D in the strong-coupling limit. The exact coupling should involve the phonon spectrum in the materials [30]. Nevertheless, using a parameter $\mu^* = 0.15$ to compare with the previous reports [11], we estimated λ_{ep} for reference in the discussion of how the superconductivity mechanism is modified when the ratio of Sn/In changes. The obtained λ_{ep} is approaching 1 at the maximum ($x = 0.3$) as in Table I. Even though we could not perform a detailed study to determine the phonon spectrum, there are several neutron-scattering measurements for single crystals of SnTe [32] and the In-doped compound $Sn_{0.8}In_{0.2}Te$ [32]. The latter experiment detects two acoustic phonon modes consistent with those of the parent SnTe [33]. The transverse optical phonon mode is linked to superconductivity, to the structural transition, and to ferroelectricity in SnTe [32], and may be expected to play an important role in the In-doped compound as well [33]. Despite the gradual change of T_c, $H_{c2}(0)$ drops drastically at $x = 0$ (InTe) as shown in Table I. Almost an order of magnitude reduction of $H_{c2}(0)$ indicates that the superconductivity is more susceptible to the applied B and the coherence length $\xi(0)$ is increased to 542.1 Å. The $H_{c2}(0)$ in $In_{1-x}Sn_xTe$ ($x \leqslant 0.5$) decreases from $H_{c2}(0) = 2$ T at $x = 0.5$ to 0.112 T for InTe. The change is rather drastic in the vicinity of InTe. It is worth noting that the $H_{c1}(0)$ in $In_{1-x}Sn_xTe$ ($0 \leqslant x \leqslant 0.5$) is increased by an order of magnitude compared to the samples synthesized in ambient pressure. It also shows that penetration depth is reduced in the mixed compounds, a behavior which is in contrast to the coherence length, which stays on the same scale. This indicates that the intermediate state where vortices penetrate into the material is larger when

Sn is doped into InTe, which may be due to the disorder effects we discussed in relation to the electronic structure calculations [34] and may be elaborated from exotic vortex states. The decrease of the Ginzburg-Landau parameter $\kappa(0)$ from 56.4 in $Sn_{0.6}In_{0.4}Te$ [13] to 2.45 in InTe suggests the material is leaning toward type-I superconductor when the In content increases. The enhancement of $H_{c2}(0)$ does not show up in InTe, indicating that the superconductivity may be different for the doped compounds even though the T_c is similar.

InTe is a good candidate to study the valence-skipping mechanism [35] due to the anomalous In valence state (In^{1+}, In^{3+}). Further detailed studies of phonon spectra and local structural modulations in single crystals would be beneficial for clarifying the possible valence-skipping superconducting mechanism. The possible change of superconducting mechanism without any structural transition demonstrates the $In_{1-x}Sn_xTe$ ($x \leqslant 0.5$) material family may be a good stage to study superconductivity. The system also shows topologically nontrivial features in the vicinity of SnTe. These features do not survive in InTe. The observed anomalous T_c modulation possibly relates to electron-phonon coupling below $x = 0.2$. It

is a promising future task to study the correlation between the exotic surface state and the change of bulk properties, which will involve single crystal growth.

In summary, we have synthesized $In_{1-x}Sn_xTe$ for x in the range of 0 to 0.5 in NaCl-type cubic structures and investigated its superconducting properties. T_c is enhanced when increasing x from 0 to 0.2 toward 0.4 to form a domelike structure of T_c. The T_c change does not correlate with the change in $\gamma(0)$, but it does correlate with the calculated $N(E_F)$. The deviation of the measured $\gamma(0)$ from the calculated $N(E_F)$ suggests that phonons could play a nontrivial role. Anomalous phonon dispersions could arise from the valence state of In or the covalency of Te in InTe and deserve further study.

[1] L. Fu, C. L. Kane, and E. J. Mele, Topological Insulators in Three Dimensions, Phys. Rev. Lett. **98**, 106803 (2007).

[2] D. Hsieh, Y. Xia, L. Wray, D. Qian, A. Pal, J. H. Dil, J. Osterwalder, F. Meier, G. Bihlmayer, C. L. Kane, Y. S. Hor, R. J. Cava, and M. Z. Hasan, Observation of unconventional quantum spin textures in topological insulators, Science **323**, 919 (2009).

[3] L. Fu and E. Berg, Odd-Parity Topological Superconductors: Theory and Application to $Cu_xBi_2Se_3$, Phys. Rev. Lett. **105**, 097001 (2010).

[4] Y. Ando, Topological insulator materials, J. Phys. Soc. Jpn. **82**, 102001 (2013).

[5] Y. S. Hor, A. J. Williams, J. G. Checkelsky, P. Roushan, J. Seo, Q. Xu, H. W. Zandbergen, A. Yazdani, N. P. Ong, and R. J. Cava, Superconductivity in $Cu_xBi_2Se_3$ and Its Implications for Pairing in the Undoped Topological Insulator, Phys. Rev. Lett. **104**, 057001 (2010).

[6] K. Matano, M. Kriener, K. Segawa, Y. Ando, and G.-Q. Zhang, Spin-rotation symmetry breaking in the superconducting state of $Cu_xBi_2Se_3$, Nat. Phys. **12**, 852 (2016).

[7] Shruti, V. K. Maurya, P. Neha, P. Srivastava, and S. Patnaik, Superconductivity by Sr intercalation in the layered topological insulator Bi_2Se_3, Phys. Rev. B **92**, 020506(R) (2015).

[8] Z. Liu, X. Yao, J. Shao, M. Zuo, L. Pi, S. Tan, C. Zhang, and Y. Zhang, Superconductivity with topological surface state in $Sr_xBi_2Se_3$, J. Am. Chem. Soc. **137**, 10512 (2015).

[9] Y. Qiu, K. N. Sanders, J. Dai, J. E. Medvedeva, W. Wu, P. Ghaemi, T. Vojta, and Y. S. Hor, Time reversal symmetry breaking superconductivity in topological materials, arXiv:1512.03519.

[10] K. Kobayashi, T. Ueno, H. Fujiwara, T. Yokoya, and J. Akimitsu, Unusual upper critical field behavior in Nb-doped bismuth selenides, Phys. Rev. B **95**, 180503 (2017).

[11] A. S. Erickson, J.-H. Chu, M. F. Toney, T. H. Geballe, and I. R. Fisher, Enhanced superconducting pairing interaction in indium-doped tin telluride, Phys. Rev. B **79**, 024520 (2009).

[12] N. Haldolaarachchige, Q. Gibson, W. Xie, M. B. Nielsen, S. Kushwaha, and R. J. Cava, Anomalous composition dependence of the superconductivity in In-doped SnTe, Phys. Rev. B **93**, 024520 (2016).

[13] G. Balakrishnan, L. Bawden, S. Cavendish, and M. R. Lees, Superconducting properties of the In-substituted topological crystalline insulator SnTe, Phys. Rev. B **87**, 140507(R) (2013).

[14] L. P. He, Z. Zhang, J. Pan, X. C. Hong, S. Y. Zhou, and S. Y. Li, Full superconducting gap in the doped topological crystalline insulator $Sn_{0.6}In_{0.4}Te$, Phys. Rev. B **88**, 014523 (2013).

[15] G. S. Bushmarina, I. A. Drabkin, V. V. Kompaniets, R. V. Parfen'ev, D. V. Shamshur, and M. A. Shakhov, Superconducting transition in SnTe doped with In, Sov. Phys. Solid State **28**, 612 (1986).

[16] L. Esaki and P. J. Stiles, New Type of Negative Resistance in Barrier Tunneling, Phys. Rev. Lett. **16**, 1108 (1966).

[17] Y. Tanaka, Z. Ren, T. Sato, K. Nakayama, S. Souma, T. Takahashi, K. Segawa, and Y. Ando, Experimental realization of a topological crystalline insulator in SnTe, Nat. Phys. **8**, 800 (2012).

[18] C. M. Polley, V. Jovic, T.-Y. Su, M. Saghir, D. Newby Jr., B. J. Kowalski, R. Jakiela, A. Barcz, M. Guziewicz, T. Balasubramanian, G. Balakrishnan, J. Laverock, and K. E. Smith, Observation of surface states on heavily indium-doped SnTe(111), a superconducting topological crystalline insulator, Phys. Rev. B **93**, 075132 (2016).

[19] J. K. Hulm, C. K. Jones, D. W. Dees, H. A. Fairbank, and P. A. Lawless, Superconducting interactions in tin telluride, Phys. Rev. **169**, 388 (1968).

[20] M. F. Mathur, D. W. Deis, C. K. Jones, and W. J. Carr Jr., Superconductivity as a function of carrier density and magnetic spin concentration in the SnTe-MnTe system, J. Phys. Chem. Solids **34**, 183 (1973).

[21] A. L. Shelankov, Mixed-valence behavior of impurities as a mechanism for superconductivity in IV-VI compounds, Solid State Commun. **62**, 327 (1987).

[22] R. Zhong, J. Schneeloch, X. Y. Shi, Z. J. Xu, C. Zhang, J. Tranquada, Q. Li, and G. D. Gu, Optimizing the superconducting transition temperature and upper critical field of $Sn_{1-x}In_xTe$, Phys. Rev. B **88**, 020505(R) (2013).

[23] C. B. Sclar, L. C. Carrison, and C. M. Schwartz, Indium telluride (II'): Transitory intermediate phase in the transformation InTe(II) to InTe(I), Science **147**, 1569 (1965).

[24] M. D. Banus, R. E. Hanneman, M. Strongin, and K. Gooen, High-pressure transitions in $A^{(III)}B^{(VI)}$ compounds: Indium telluride, Science **142**, 662 (1963).

[25] T. Chattopadhyay, R. P. Santandrea, and H. G. von Schnering, Temperature and pressure dependence of the crystal structure of InTe: A new high pressure phase of InTe, J. Phys. Chem. Solids **46**, 351 (1985).

[26] K. Koepernik and H. Eschrig, Full-potential nonorthogonal local-orbital minimum-basis band-structure scheme, Phys. Rev. B **59**, 1743 (1999); http://www.FPLO.de

[27] K. Koepernik, B. Belicky, R. Hayn, and H. Eschrig, Self-consistent LCAO-CPA method for disordered alloys, Phys. Rev. B **55**, 5717 (1997).

[28] J. P. Perdew, K. Burke, and M. Ernzerhof, Generalized Gradient Approximation Made Simple, Phys. Rev. Lett. **77**, 3865 (1996).

[29] N. R. Werthamer, E. Helfand, and P. C. Hohenberg, Temperature and purity dependence of the superconducting critical field, H_c2. III. Electron spin and spin-orbit effects, Phys. Rev. **147**, 295 (1966).

[30] W. L. McMillan, Transition temperature of strong-coupled superconductors, Phys. Rev. **167**, 331 (1968).

[31] P. B. Allen, *Handbook of Superconductors*, edited by Charles P. Poole, Jr., (Academic Press, New York, 1999).

[32] C. D. O'Neil, D. A. Sokolov, A. Hermann, A. Bossak, C. Stock, and A. D. Huxley, Inelastic x-ray investigation of the ferroelectric transition in SnTe, Phys. Rev. B **95**, 144101 (2017).

[33] Z. Xu, J. A. Schneeloch, R. D. Zhong, J. A. Rodriguez-Rivera, L. W. Harriger, R. J. Birgeneau, G. D. Gu, J. M. Tranquada, and G. Xu, Low-energy phonons and superconductivity in $Sn_{0.8}In_{0.2}Te$, Phys. Rev. B **91**, 054522 (2015).

[34] M. P. A. Fisher, Vortex-Glass Superconductivity: A Possible New Phase in Bulk High-T_c Oxides, Phys. Rev. Lett. **62**, 1415 (1989).

[35] C. M. Varma, Missing Valence States, Diamagnetic Insulators, and Superconductors, Phys. Rev. Lett. **61**, 2713 (1988).